JOURNAL OF RHEOLOGY

The correlation of experimental surface extrusion instabilities with numerically predicted exit surface stress concentrations and melt strength for linear low density polyethylene

Rulande Rutgers and Malcolm Mackley

Citation: J. Rheol. **44**, 1319 (2000); doi: 10.1122/1.1319176
View online: http://dx.doi.org/10.1122/1.1319176
View Table of Contents: http://www.journalofrheology.org/resource/1/JORHD2/v44/i6
Published by the The Society of Rheology

The correlation of experimental surface extrusion instabilities with numerically predicted exit surface stress concentrations and melt strength for linear low density polyethylene

Rulande Rutgers[a)]

Department of Chemical Engineering, University of Queensland, Brisbane 4072, Queensland, Australia

Malcolm Mackley

Department of Chemical Engineering, University of Cambridge, Pembroke Street, Cambridge CB2 3RA, United Kingdom

(Received 30 November 1999; final revision received 17 August 2000)

Synopsis

Experimental data on the onset and magnitude of surface instabilities are reported for two grades of linear low density polyethylene. Numerical simulation of the flow is presented and the magnitudes of surface stress concentrations established. The onset of experimentally observed surface instabilities is then correlated with the magnitude of the surface stress concentrations at the exit and also with the melt strength of the polymer. © *2000 The Society of Rheology.*
[S0148-6055(00)01106-8]

I. INTRODUCTION

Linear low density polyethylene (LLDPE) is particularly sensitive to extrusion surface instabilities, which have most recently been reported in papers by Piau *et al.* (1995), Wang *et al.* (1996), Venet and Vergnes (1997), and Mackley *et al.* (1998a, 1998b). Surface instabilities for LLDPE are generally described as a fine scale high frequency small amplitude extrudate distortion or surface roughness and most previous studies characterize the instability in terms of amplitude and wavelength of ridges on the cooled extrudate [see for example Tzoganakis *et al.* (1993); Wang *et al.* (1996). Kurtz (1993), Joseph and Liu (1996), and Mackley *et al.* (1998a, 1998b)] have highlighted the three-dimensional nature of the distortion, and described it as ''chevrons'' or ''waves.''

Surface instabilities have been distinguished from other extrusion instabilities which lead to a fluctuating pressure difference in the bulk flow [e.g., Tordella (1963); Cogswell (1977)] and in the case of surface instabilities little experimental data is available on the flow or stress field that occurs near the surface [e.g., Sornberger *et al.* (1987)].

Although general agreement on most experimental observations has now been achieved with respect to the conditions for the onset of surface instabilities, there are still conceptual differences in terms of the mechanistic interpretation of the effect. A number of models and mechanisms have been proposed, which can be roughly classified into

[a)]Author to whom correspondence should be addressed; electronic mail: r.rutgers@cheque.uq.edu.au

three sections; involving (a) *transition of the wall boundary condition* such as the stick–slip mechanism first proposed by Vinogradov *et al.* (1972); (b) *rheological effects near the wall*, which may indicate a constitutive instability; or (c) *crack formation at the exit* due to extensional stresses as first suggested by Cogswell (1977). Mechanisms involving instabilities in the entry region were eliminated at an early stage due to the overriding experimental evidence of the importance of exit region. Experimental evidence thusfar has also failed to support a mechanism involving cavitation at the wall near the exit as suggested by Tremblay (1991). A brief review of the three mechanisms is given in the next three subsections of this paper.

A. Transition of the wall boundary condition

The frequently made, yet controversial, connection between a change in slope in the flow curve and the onset of surface instabilities has resulted in the proposal of various mechanisms that involve slip at the wall. The slip mechanism first proposed by Hill *et al.* (1990) and further researched most recently by Ghanta *et al.* (1999) predicts the onset of surface instabilities and the slip velocity on the basis of wall–polymer bonding strength determined from peeling experiments for various materials. Dynamics have been modeled with various slip laws [e.g., Georgiou and Crochet (1994); Hatzikiriakos and Kalogerakis (1994); Shore *et al.* (1997)], which generally yield some form of waviness of the extrudate, but also in small pressure oscillations, for which experimental evidence has not yet been established. Hatzikiriakos and Dealy (1993) explore the site of the instability, demonstrating that the slip boundary condition originates at the exit, due to low pressures, and travels upstream with increasing shear rate. The slip model predicts increasingly high elongation rates near the exit with increasing shear rates which, it is suggested, induce melt rupture. Kurtz (1984) also proposes a combination of melt rupture and localized wall slip near the exit. The role of the slip wall boundary condition in alleviating as opposed to contributing to surface instabilities has also been researched thoroughly, e.g., by Hatzikiriakis and Dealy (1993), Piau *et al.* (1995), and by the investigation of instabilities in brass dies by Ramamurthy (1986) and most recently by Ghanta *et al.* (1999).

B. Rheological effects near the wall

A number of authors have considered short wave instabilities based on a region in the flow curve characteristic for the presence of two rheologically differing phases [e.g., Huseby (1966); McLeish (1987); Renardy (1995); Wilson and Rallison (1997)]. Growth of this type of instability can only occur if part of the flow curve has a negative slope [McLeish (1987)] which is not the case for LLDPE in the region of the flow curve where surface instabilities occur. Joseph and Liu (1996) have modeled the experimentally observed sharp wave fronts in polymer melt extrusion using a ''flying core'' model. Koopmans and Molenaar (1996) use a relaxation–oscillation mechanism to combine the nonmonotonic flow curve with polymer melt compressibility to model small pressure and velocity oscillations in the flow curve branch before the discontinuity that marks the spurt regime. Experimental evidence for these small fluctuations in velocity and pressure has not been gathered in the regime where surface instabilities occur for LLDPE.

Wang *et al.* (1996); [Barone *et al.* (1998)] and Wang and Plucktaveesak (1999) propose an ''unstable melt/wall boundary condition'' which involves periodic (adhesive) disentanglement of a layer of polymer chains grafted at the wall from the bulk of the material. This cyclical entanglement–disentanglement transition is dependent on chain dynamics and only happens near the exit but within the capillary section, where stresses

are high. The length of the section of the die wall that is occupied by the grafted chains involved in this instability is not specified. The amplitude growth of the instability is attributed to bulk (cohesive) disentanglement when a critical stress is reached further away from the wall. The periodic fluctuation between coil and stretch states leads to a quasiperiodic perturbation of the extrudate swell. The onset conditions for this reversible local stick–slip transition is an ''extensional stress field originating from the boundary discontinuity'' at a wall shear stress below the critical wall shear stress for the onset of global slip. Absence of surface instabilities on polytetrafluoroethylene coated dies is attributed to the absence of adsorbed chains that enable the oscillatory boundary condition.

Experimental evidence of the entanglement–disentanglement transition through coextruded ordinary (core) and pigmented (annular) polyethylene [Wang and Plucktaveesak (1999)] has previously been ascribed by Cogswell (1977) to semiperiodic surface cracking. Wang and Plucktaveesak (1999) suggest that the extrudate is black during slip and white when the black layer sticks at the wall. However, the thickness of the pigmented layer that would (indefinitely) stick to the wall under no-slip conditions such as to expose a perfectly white extrudate would need to be the order of a monolayer, unless a constitutive instability occurred which would cause the core material to slip along the layer of black material at the wall. As such a constitutive instability is not proposed by Wang and Plucktaveesak (1999) it appears more plausible that cracking of the black skin explains the periodic exposure of pure white extrudate.

C. Crack formation at the exit

As discussed in the previous section Cogswell (1977) and Wang and Plucktaveesak (1999) provide experimental proof of a visibly discontinuous surface layer when surface instabilities occur, suggesting that cracking of the material occurs. Piau *et al.* (1995); El Kissi *et al.* (1997) extensively explored the rupture mechanism by observing the instability as the extrudate exits, rather than investigating the cooled extrudate. In order to produce the sharp sawtooth-like extrudate profile such as that observed by Venet and Vergnes (1997) rupture appears to be the most likely mechanism, as opposed to chain relaxation dynamics, waviness between two rheologically different material fractions, or oscillating boundary conditions. The rupture mechanism is an exit phenomenon, unrelated to unstable conditions inside the die or upstream from the capillary or slit.

Although Barone *et al.* (1999) observe that all extrusion instabilities occur at wall shear stress levels (of order 0.15–0.4 MPa) below the melt strength of the material, in this paper we argue it is the extensional stress level that is the critical variable for melt strength and hence rupture. At the exit of the die, the flow singularity extensional stress will be expected to reach values above the critical stress level for melt failure. An analysis on ''bouncy putty'' [Cogswell (1977)] showed that a critical stretch rate, which is highest immediately after the die exit in absence of slip at the wall, could be identified and related to the tensile rupture stress of the material.

Quantification of the critical conditions and simulation of the dynamics of the mechanism has very recently been attempted by Venet (1996). Through numerical simulations Venet intends to relate the wavelength of the instability to the length of a critical elongational stress zone, whereas the authors of this paper have thusfar focused on the amplitude of the instability in relation to the magnitude of the extensional stress peak observed numerically at the extrudate surface at the die exit [Mackley *et al.* (1998a, 1998b)].

The above discussion of the various mechanisms demonstrates that it has been difficult to develop a critical experiment which is able to discriminate definitively between the

TABLE I. Rheological parameters of the melts.

λ_i (s)	LL09 [g_i(Pa)]	LL05 [g_i(Pa)]
2.00×10^{-3}	1.56×10^{5}	2.30×10^{5}
9.38×10^{-3}	1.70×10^{5}	2.48×10^{5}
4.40×10^{-2}	5.40×10^{4}	9.89×10^{4}
2.06×10^{-1}	1.92×10^{4}	3.71×10^{4}
9.69×10^{-1}	3.73×10^{3}	8.61×10^{3}
4.54×10^{0}	6.86×10^{2}	1.60×10^{3}
2.13×10^{1}	1.55×10^{2}	2.74×10^{2}
1.00×10^{2}	3.39×10^{1}	9.11×10^{1}
k (−)	0.24	0.25

various proposed mechanisms [see also Watson (1999a; 1999b) Barone *et al.* (1999)]. Most of the mechanisms described above require either a critical shear stress or extensional stress, and each mechanism may explain the variation in the severity of surface instability as a result of a modified stress field. However, it is suggested in this paper that only a rupture mechanism could explain a correlation between surface instability and melt strength. The region of the extrudate where the extensional stress level reaches the melt strength of the material would be prone to local rupture. Reducing the exit extensional stress below the melt strength on the other hand, will help prevent the occurrence of surface instabilities. This paper focuses on this particular hypothesis, however the authors do not exclude the possibility that other factors, such as the presence or absence of slip or a critical strain rate, may also affect the onset or severity of the instability.

This paper investigates the extensional stress levels in the exit region of the die by means of numerical simulation, in order to establish if there is a connection between the local stress conditions, the onset and development of surface instabilities, and melt failure in tensile tests. The characterization of the surface instability and the validation of the numerical simulation are discussed. The onset and development of surface instability as a function of flow rate, temperature, molecular mass, and die geometry is investigated and a correlation with underlying local stress conditions established.

II. MATERIALS AND METHODS

A. Rheological characterization

The materials studied were two C6 LLDPE grades, LL09 and LL05, supplied by BP Chemicals, with melt flow indices (MIs) of 0.9 and 0.5, respectively. The molecular masses determined from gel permeation chromatography measurements were $M_w = 118\times10^3$ and $M_w = 140\times10^3$, respectively, with comparable molecular mass distributions (MMD) of order 4 ($M_w/M_n = 4.23$ and 3.93, respectively). The rheological behavior of the materials was modeled using a KBKZ integral constitutive equation with a Wagner type irreversible damping factor [Wagner (1976; 1979)]. The equation and the experimental determination of the parameters for this model was described previously [Mackley *et al.* (1998a, 1998b)]. The relaxation spectrum covers relaxation times of 10^{-3}–10^{2} s. The spectra (in terms of relaxation times λ_i and partial elasticities g_i) and damping factors (k) obtained in simple shear are given in Table I, LL05, the lower MI material with the slightly higher molar mass and narrower MMD, exhibits significantly higher elasticities than LL09. The materials were processed in a manner described by Mackley *et al.* (1998a and 1998b).

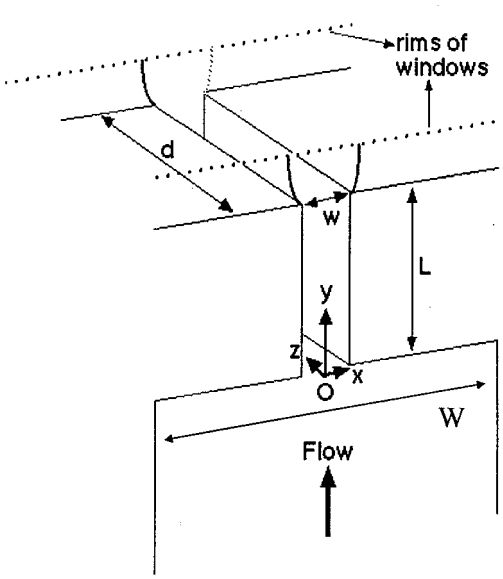

FIG. 1. Schematic of die geometry. Flow from bottom to top. Die depth $d = 15$ mm, $L =$ slit length, $w =$ gap width. Dotted lines indicate the edges of the cutoff windows.

B. Characterization of the instability

The qualitative characteristics of the extrudate were determined through scanning electron microscopy, and the observed semiperiodic wave-like distortion was quantified using a number of Taylor Hobson stylus surface profile measurement instruments (Form Talisurf+ and Form Talysurf 120-L).

The extrudate roughness in the direction of the flow was expressed in terms of R_{zDIN} as a measure of amplitude, which is the average height difference between the five highest peaks and the five lowest valleys in the sampling length, subsequently averaged over the total assessment length (five times the sampling length). The sampling length is a custom-defined cutoff length in order to filter out any waviness in the extrudate. The nondestructive effect of the stylus on the extrudate and the applicability of the measurement technique given the dimensional characteristics of the extrudate and the stylus was verified; routine calibrations and 3–5 repeat measurements on each sample were carried out to obtain the presented results.

C. Numerical simulation of the flow

The flow studied is an abrupt (180°) contraction planar flow with a free surface die swell and is shown schematically in Fig. 1. The die geometries studied are given in Table II. Here $w =$ slit gap width, $d =$ depth, $L =$ slit length, and $W/w =$ contraction ratio. The stainless steel dies were polished to an average roughness of approximately $R_a = 1\ \mu$m.

For the numerical simulation of the steady flow, the commercial finite element package Polyflow was used. Three meshes were used at 920, 1937, and 2852 elements, respectively. The meshes were refined near the entry and exit corners, such that the element immediately at the wall at the exit were 16 μm by 16 μm, 8 μm by 8 μm, and 4 μm by 4 μm, respectively. Quadratic interpolation was used for velocities and linear

TABLE II. Die dimensions and surface finish (in terms of average roughness R_a).

Die No.	w (mm)	L (mm)	d (mm)	W/w (−)	R_a (μm)
1	1.125	8.03	15.00	13.3	0.5
2	1.125	2.00	15.02	13.3	—
3	1.200	23.82	15.03	12.5	0.5
4	2.050	8.00	15.01	6.5	1.25
5	2.47	8.10	15.00	6.1	—
6	1.200	0.5[a]	15.01	12.5	—

[a]Orifice-type insert with a 120° exit angle.

discontinuous interpolation for pressure. The boundary conditions were fully developed flow 25 mm upstream from the slit entrance; symmetry along the center plane; zero slip velocity at the wall; and an 80 mm long free surface with zero force at the outlet. The effect of a finite slip velocity was studied [Rutgers (1998)] but is not discussed here.

The numerical simulation of the flow was validated by comparing numerical global stress fields and centerline principal stress difference (PSD) profiles with the experimental values from stress birefringence measurements [see Mackley *et al.* (1998a, 1998b)]. Further verification included pressure difference, centerline velocities, and die swell [Rutgers (1998)]. The match was found to be good, with discrepancies between the numerical and experimental maximum entry stress along the centerline of order 1% and 20% for LL09 and LL05, respectively. These discrepancies lie within the estimated experimental and numerical error of 9% and 12%, respectively [Rutgers (1998)], although it may be argued that the elongational behavior of LL05 is less well predicted than that of LL09. Comparisons between experimental and numerical wall shear stress are given in Fig. 2. For LL09 the experimental (Bagley end-corrected) and predicted wall shear stress are identical. The prediction for LL05 was slightly less accurate.

The good matching between our numerical simulation and the global experimental stress birefringence measurements gives us confidence that the simulation reliably predicts the overall flow behavior of the LLDPEs under test. From this position we then

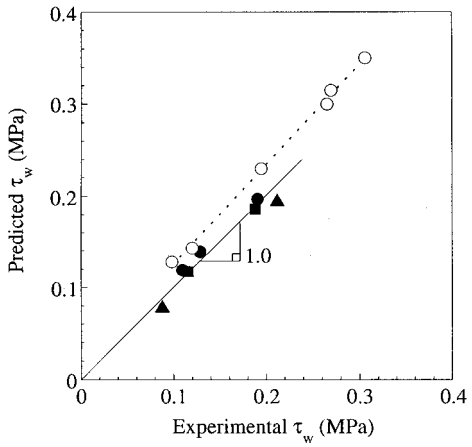

FIG. 2. Comparison between simulated and experimental (Bagley end-corrected) wall shear stress at $T = 180\,°C$: (open symbols) LL09; (closed symbols) LL09; (circles) die length $L = 8$ mm; (triangles) $L = 2$ mm; (squares) $L = 23$ mm.

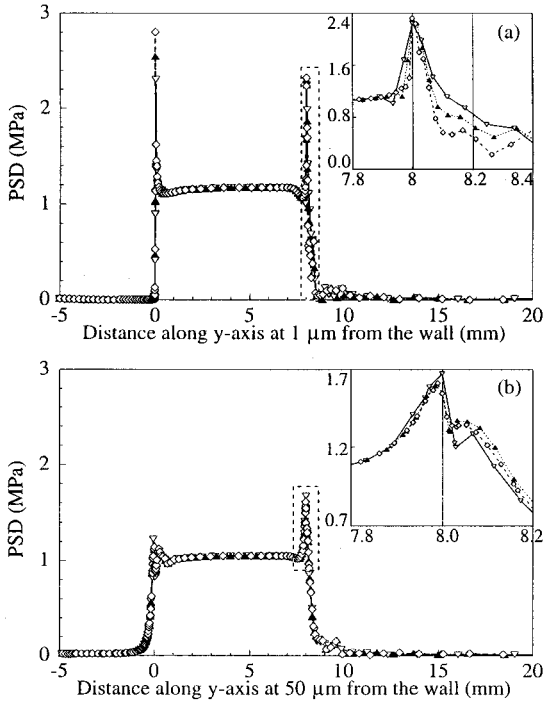

FIG. 3. Sensitivity of the prediction to mesh refinement for LL05 at 180 °C and an apparent shear rate of 92.5 s^{-1}: (a) PSD along streamline at 1 μm from wall; (b) PSD along streamline at 50 μm from wall: (continuous line, open triangles) coarse mesh; (dotted line, closed triangles) medium mesh; (dashed line, open diamonds) refined mesh.

move forward and use the simulations to predict stress fields near the wall and surface at the exit, which cannot at present be obtained using our available experimental techniques.

For the purpose of the investigation of the trends in the exit stresses, we wish to study a streamline close to the wall, but are limited by the length scales of: (a) the wall roughness of the die, (b) validity of continuum mechanics, and (c) the numerical artifact of unphysically large stress values for increasingly small elements at the exit singularity.

It is noted that the dies used in the experiment have an average surface roughness of order $R_a = 1$ μm. An ideal saw-tooth profile with this average roughness would have peak to valley distances of 4 μm. Assuming a factor of 10 is suitable, the wall cannot be considered smooth at length scales below 40 μm.

The average end-to-end distance of an individual polymer molecule with a molecular mass of 100 000 under θ-conditions is of order 30 nm, and its contour length is of order 900 nm. A distance of 30 μm from the wall would represent a factor of 1000 and 30 with respect to θ-conditions and fully extended configuration, respectively. This is considered reasonable for the validity of continuum mechanics.

Mesh sensitivity was investigated by comparing the solutions of the global stress field, the centerline stresses and velocities, the transverse stress profile across the slit at the exit, and the stress profile along streamlines close to the wall. Figure 3 shows a PSD profile obtained with the three meshes, along streamlines 1 and 50 μm from the wall. The simulation confirms the experimentally observed important stress concentration at the die exit, which is largest closest to the wall. It is noted that with the three meshes the same

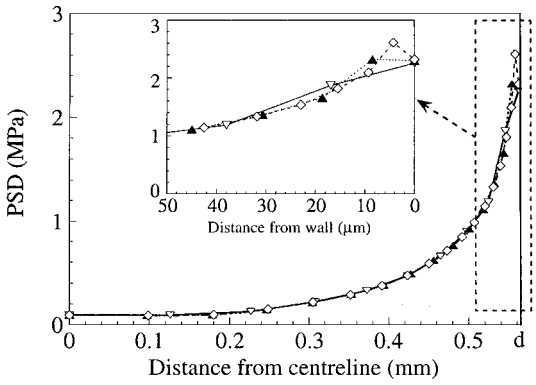

FIG. 4. Sensitivity of the PSD across the slit at the exit to mesh refinement: (continuous line, open triangles) coarse mesh; (dotted line, closed triangles) medium mesh; (dashed line, open diamonds) refined mesh.

magnitude of the stress peak is predicted within 10%, both at the streamline at 1 μm from the wall and at 50 μm from the wall. Some discrepancies are observed in the wake of the stress peak at 1 μm from the wall. Figure 4 shows the simulation of the PSD across the slit at the die exit. The transverse stress profile across the die exit demonstrates that a difference in the solution between the three meshes only occurs in the element closest to the wall. This is a numerical artifact due to and confined to the singularity at the exit. Indeed the more refined the mesh, the higher the numerically predicted stress will be in the one node adjacent to the wall. It may however be concluded that mesh independence of the simulation was obtained outside the element immediately adjacent to the wall, which in this case was 16 μm for the coarsest mesh. This is below the length scales for continuum mechanics and smooth wall assumptions and hence satisfactory for this discussion. The criteria for convergence (relative change in the velocity field and the streamlines $< 10^{-3}$) were met for each simulation. Unfortunately it was impossible to experimentally verify the prediction close to the singularity, due to lack of experimental resolution.

We consider the streamline at 50 μm from the wall for the discussion below. In light of the above discussion on suitable length scales and convergence, this is a very conservative distance from the exit, while still allowing meaningful correlations with the developed surface instability discussed in this paper, which has an amplitude of the order of magnitude of 10–100 μm at the exit of the die. It is important to recall from Fig. 4 that closer to the surface at the exit of the die the PSD is greater than that observed at the streamline at 50 μm from the wall: If a critical value of PSD is reached with increasing shear rate this value will first be reached at the surface and then further into the bulk of the material.

D. Rheotens measurements of melt rupture stress

The critical stress level for melt rupture in uniaxial elongation was determined through a modified Rheotens experiment [Wagner *et al.* (1997)], where the extrudate from a capillary rheometer at constant volumetric flow rate and average exit velocity v_0 is stretched under the action of a constant tensile force F, and hence a variable draw ratio $V = v/v_0$. The measured tensile force is constant throughout the length of the elongated extrudate, and the stress is obtained from

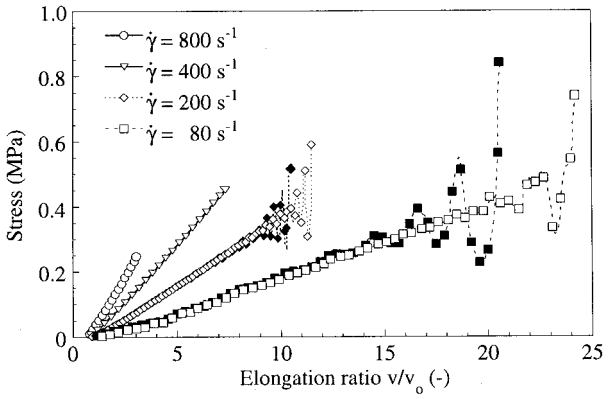

FIG. 5. Rheotens curves. Stress as a function of draw ratio for LL09 at 180 °C for various shear rates in the capillary.

$$\sigma = \frac{F}{A} = \frac{FV}{A_0}, \tag{1}$$

where A and A_0 are the surface areas of the local cross section of the extrudate and of the cross section of the capillary exit, respectively. The failure stress is defined as the last stress measured before rupture of the extrudate.

Figure 5 shows typical Rheotens curves for LL09 at various capillary shear rates. It is apparent that draw resonance occurs at the low shear rates, which may affect the accuracy of the measured rupture stress at these rates [Wagner *et al.* (1997)].

III. RESULTS AND DISCUSSION

A. Experimental study of the onset and growth of the instability

1. Dependence on flow rate and temperature

Industrial experience and previous work indicates that surface instabilities appear and grow with increasing flow rate, and that increasing the temperature reduces the effect. Figure 6 shows the amplitude of the extrudate roughness of LL09 as a function of scaled wall shear stress for extrusions at a range of temperatures between 140 and 200 °C. The scaled wall shear stress is defined as $\tau_w T_0 / T$ [Venet and Vergnes (1997)] at $T_0 = 180\,°\mathrm{C}$. The shear stress is determined from the overall pressure difference along the die, corrected for the end pressure differences using a shear rate dependent Bagley correction.

The curves at various temperatures form an exponential ''master curve'' of amplitude against scaled wall shear stress. Not shown here is the linear dependence between amplitude and wavelength of the distortion, with the wavelength a factor of order 10 larger than the amplitude, dependent on haul-off ratio.

2. Dependence on molecular mass

Although the higher molecular mass grade is known in the industry to show surface instability at much lower processing rates, the stress dependence of the surface instability is comparable for both materials (see Fig. 7). The observations discussed here all point to the wall stress being the single most important factor concerning the onset and development of extrusion surface instability.

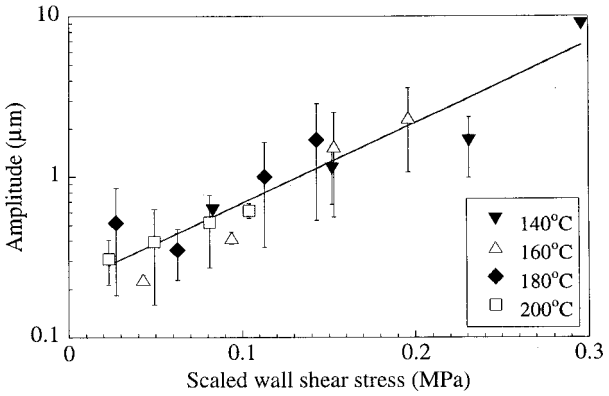

FIG. 6. Amplitude of the extrudate roughness of LL09 as a function of scaled wall shear stress $\tau_w T_0 / T$ at $T_0 = 180\,°C$: (closed reversed triangles) 140 °C; (open triangles) 160 °C; (closed diamonds) 180 °C; (open squares) 200 °C.

3. Dependence on die geometry

Both the dependence on die length and gap width were investigated. The range of dies investigated includes lengths from 2 to 24 mm for a 1 mm gap width, and die gaps of 1, 2, and 2.5 mm for an 8 mm long die. Confirming findings by Venet and Vergnes (1997), the die length does not have a significant or systematic effect on the severity of the surface distortion, and is not shown here.

The die gap on the other hand does affect the amplitude of the instability (Fig. 8). Here the effect of contraction ratio on the Bagley correction is assumed negligible [Bagley (1957)]: The same shear rate dependent end correction is used for the three die gaps.

B. Correlation between numerically predicted local stress conditions and the onset of instabilities

1. Numerical study of flow conditions near the die exit

Figure 9 shows the tracking of stresses [Fig. 9(a)] and deformation rates [Fig. 9(b)] as a function of distance along a streamline at 50 μm from the wall. Important peaks in

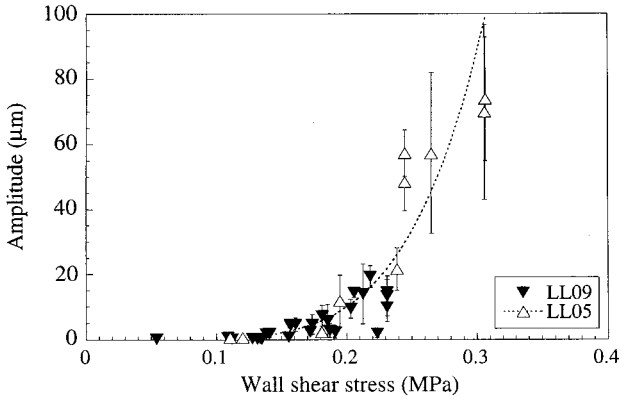

FIG. 7. Amplitude of surface instability of LL09 and LL05 extruded from die 1 at 180 °C as a function of wall shear stress.

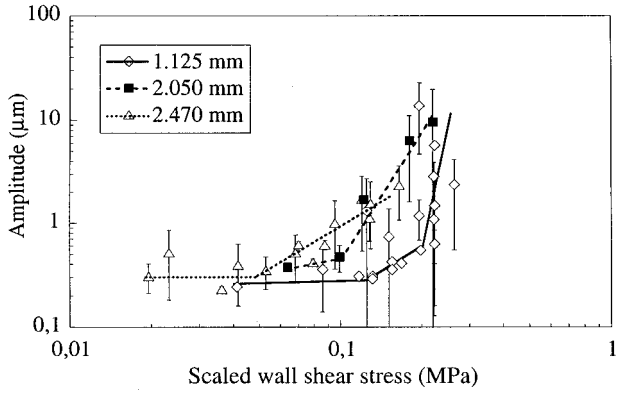

FIG. 8. Amplitude of surface instability of LL09 extruded at 152–212 °C as a function of die gap width: (open diamonds) $w = 1.125$ mm; (closed squares) $w = 2.05$ mm; (open triangles) $w = 2.47$ mm.

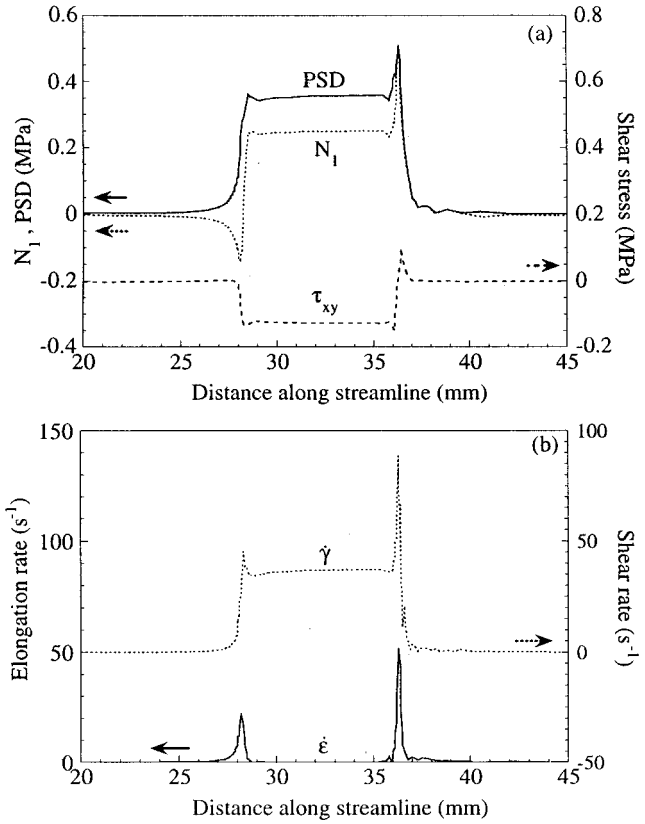

FIG. 9. Tracking of stresses (a) and rates (b) along the streamline at 50 μm from the wall for LL09 in die 1 at 180 °C and a flow rate of 1.1×10^{-7} m^3/s. (N_1) first normal stress difference; (PSD) principal stress difference; ($\dot{\epsilon}$) extension rate; ($\dot{\gamma}$) shear rate.

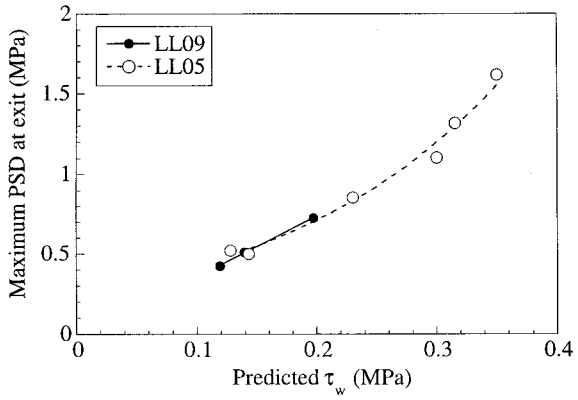

FIG. 10. Simulated PSD exit peak for two LLDPEs at 180 °C vs simulated wall shear stress: (closed symbols) LL09; (open symbols) LL05.

extensional stress, shear rate, and extension rate are observed at the exit of the die where they are related to the transition from a zero slip velocity at the wall to a free surface velocity where die swell occurs. These peaks are of greater magnitude than the corresponding peaks seen at the entry of the slit.

Figure 10 shows that the PSD exit peak increases with shear stress for both LLDPEs, and that the shear stress dependence of this peak is identical for both materials (Fig. 10). This correlates directly with the trends of the amplitude of the surface instability (Fig. 7). In the relevant shear stress range for extrusion surface instabilities (0.15–0.3 MPa), the exit peak of the PSD is shown to reach levels of order 0.7–1.3 MPa in the streamline at 50 μm from the surface.

Figure 11 shows the die geometry dependence of the exit peak for the PSD. The independence of die length found for the amplitude of the extrudate surface distortion is also reflected in the amplitude of the PSD exit peak. The PSD peak is more important for the wider die gap at comparable shear stresses. The elongational stress at the exit is a result of the change in the velocity profile at the exit of the die. This transition is greater as the average velocity is greater. Therefore the extensional stress peak increases with increasing flow rate (i.e., increasing shear rate and shear stress). In a wider die gap a

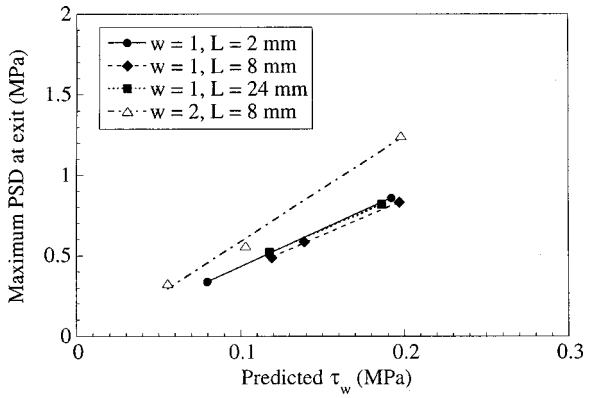

FIG. 11. Simulated PSD exit peak for LL09 at 180 °C as a function of slit geometry.

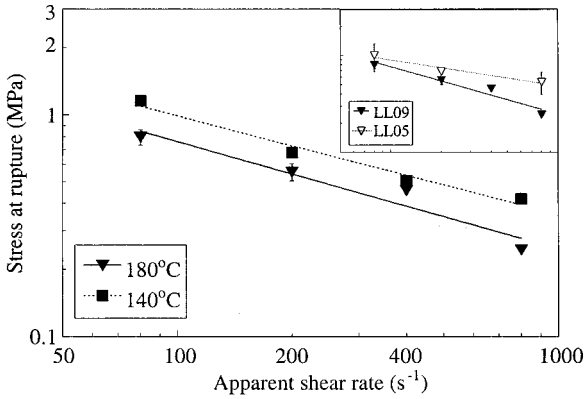

FIG. 12. Rheotens critical melt rupture stress as function of apparent shear rate in the upstream capillary for LL09 (closed symbols) at 180 °C (triangles) and at 140 °C (diamonds) and compared to LL05 (open symbols) at 180 °C (inset)

greater average velocity is required to achieve a shear stress comparable to that obtained in a small die gap. The greater elongational stress peak for a wider die gap at equal shear stress is hence due to the higher flow rate which results in a greater transition at the exit.

It was previously shown that the instability amplitude was also greater for wider die gaps at comparable shear stresses (Fig. 8). This result suggests that the instability is dependent on the elongational exit stress, independently of the wall shear stress. This represents important experimental evidence that uncouples the elongational stress dependence of the instability from its shear stress dependence.

2. Experimental study of Rheotens extensional melt rupture

The critical stress for melt rupture as a function of shear rate in the upstream capillary is given in Fig. 12. Melt rupture stress is not given as a function of shear stress as the Rheotens apparatus used did not provide pressure measurements. At shear rates of order 100 s^{-1} (representative for surface instabilities) the critical stress for melt rupture is of order 0.7–1 MPa. Both the temperature dependence (Fig. 12) and the molecular mass dependence (inset) are expected: A lower temperature and a higher molecular mass both increase the stress required for rupture to occur.

3. Instability map

The comparison between the critical stress for melt failure in uniaxial experiments and the level of the PSD exit peak during extrusion, is set out against apparent slit wall shear rate in Fig. 13. It is clear that the exit stress levels in slit extrusion reach critical levels that would lead to melt rupture in uniaxial stretching experiments.

Figure 13 maps out the maximum PSD stress peak predicted on the ''50 μm'' contour as a function of apparent wall shear rate in the slit: For example, data point A corresponds to a simulated maximum PSD of 0.5 MPa for a wall shear rate of 33 s^{-1}. For the two polymers tested there appeared to be a linear dependence between wall shear rate and maximum PSD at the exit.

For each flow condition the level of experimentally observed surface roughness is indicated: Smooth extrudates are marked by a continuous line while extrudates with surface roughness are signified by a dashed line. A transition from smooth to rough appears to occur in the region where the maximum simulated PSD is of order 1 MPa.

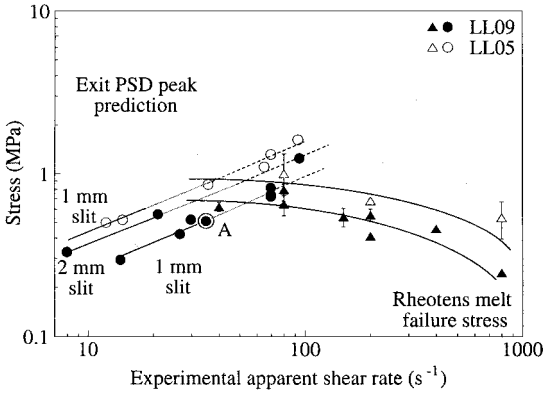

FIG. 13. Surface instability map for LL09 (closed symbols) and LL05 (open symbols) at 180 °C. Circles indicate the simulated peak values of PSD at the die exit, triangles indicate the Rheotens rupture stress. The lines linking the PSD data indicate the level of surface extrudate roughness: (continuous line) stable flow, (dotted) 1–10 μm, (dashed) 10–100 μm.

Rheotens data are also presented on the instability map shown in Fig. 13. In this case the ''melt strength'' is plotted as a function of the upstream capillary wall shear rate. From inspection of Fig. 13 it appears that the onset of extension surface instabilities occurs when the maximum exit PSD is close to the melt strength of the polymer, and from this observation we conclude that it is the maximum PSD at the die exit and the material's melt strength that controls the onset of surface instability for LLDPE. An increase in gap width or in molecular mass shifts the curve of maximum PSD to lower shear rates, thus explaining why the critical condition for local melt rupture is reached at a lower shear rate in these cases.

Plausibly, periodicity of the crack formation and growth, can be envisaged based on the following scenario: Cracks initiate at the surface as the critical level is reached; the exact locations of initiation will be dependent on inhomogeneities in polymer and die surface; and the cracks may travel sidewards and into the bulk of the material until locations are reached where the stress level is somewhat below the critical stress, as propagation requires less energy than initation. Concurrently, as soon as a crack forms, the stress level in the surrounding material decreases as the crack relieves the extensional force exerted on the material. When the crack stops, the stress level will build up again.

IV. CONCLUSIONS

The onset and growth of extrusion surface instability has been shown to correlate to the level of exit tensile stresses at the surface of the extrudate at the exit of the die. Critical stress levels for melt rupture were quantified through Rheotens uniaxial extension experiments, and were numerically shown to be reached at the exit of the die. The extensional stress peak at the exit of the die is highest at the surface, and decreases into the bulk of the material. Thus, with increasing shear rate, a larger surface layer is susceptible to crack growth, as material further into the bulk reaches the critical stress level of order 1 MPa for LLDPE. As the critical extensional stress level is reached, periodical crack formation occurs and the depth of the cracks is correlated to the thickness of the layer of material in which the stress exceeds the critical level. It has been shown that molecular mass dependence, temperature dependence, and die geometry dependence of

the extrusion surface instability can thus be explained in terms of the magnitude of the extensional stress peak at the die exit.

On the basis of these findings prediction of extrusion surface instabilities for polymer-die geometry combinations can be carried out through numerical simulation of the PSD peaks at the exit of the die and experimental determination of the melt strength. Increasing the melt strength of the material, or decreasing exit stress level experienced by the material, either through die design or polymer design, are the tools to explore to delay the onset of surface instabilities. The suppression of extrusion surface instabilities through die exit design and wall slip was elsewhere shown to be consistent with this theory [Rutgers (1998)]. It is important to establish whether the proposed correlation among surface instabilities, critical exit stress, and melt strength is sufficient to interpret documented experimental evidence or if additional factors play a role, such as proposed by Kurtz (1984), Ramamurthy (1986), Hatzikiriakos and Dealy (1994), Barone *et al.* (1998), and Ghanta *et al.* (1999).

ACKNOWLEDGMENTS

The authors are grateful to the EPSRC and BP Chemicals for financial support and materials, and to D. G. Gilbert from BP Chemicals and A. D. Goublomme from Polyflow S. A. for insightful discussions. Rheotens experiments and related knowledge were kindly provided by A. Bernnat and M. H. Wagner. Mesh sensitivity analysis was carried out by N. Clemeur. The surface profile measurement equipment was at our disposal provided by Taylor Hobson Pneumo.

References

Bagley, E. B., ''End corrections in the capillary flow of polyethylene,'' J. Appl. Phys. **28**, 624–627 (1957).

Barone, J. R., N. Plucktaveesak, and S. Q. Wang, ''Interfacial molecular instability mechanism for sharkskin phenomenon in capillary extrusion of linear polyethylenes,'' J. Rheol. **42**, 813–832 (1998).

Barone, J. R., N. Plucktaveesak, and S. Q. Wang, ''Author's response,'' J. Rheol. **43**, 247–251 (1999).

Cogswell, F. N., ''Stretching flow instabilities at the exits of extrusion dies,'' J. Non-Newtonian Fluid Mech. **2**, 37–47 (1977).

El Kissi, N., J.-M. Piau, and F. Toussaint, ''Sharkskin and cracking of polymer melt extrudates,'' J. Non-Newtonian Fluid Mech. **68**, 271–290 (1997).

Georgiou, G. C. and M. J. Crochet, ''Time-dependent compressible extrudate-swell problem with slip at the wall,'' J. Rheol. **38**, 1745–1755 (1994).

Ghanta, V. G., B. L. Riise, and M. M. Denn, ''Disappearance of extrusion instabilities in brass capillary dies,'' J. Rheol. **42**, 435–442 (1999).

Hatzikiriakos, S. G. and J. M. Dealy, ''Effects of interfacial conditions on wall slip and sharkskin melt fracture of HDPE,'' Int. Polym. Process. **8**, 36–43 (1993).

Hatzikiriakos, S. G. and N. Kalogerakis, ''A dynamic slip velocity model for molten polymers based on a network kinetic theory,'' Rheol. Acta **33**, 38–47 (1994).

Hill, D. A., T. Hasegawa, and M. M. Denn, ''On the apparent relation between adhesive failure and melt fracture,'' J. Rheol. **34**, 891–918 (1990).

Huseby, T. W., ''Hypothesis on a certain flow instability in polymer melts,'' Trans. Soc. Rheol. **10**, 181–190 (1966).

Joseph, D. D. and Y. J. Liu, ''Steep wave fronts on extrudates of polymer melts and solutions,'' J. Rheol. **40**, 317–319 (1996).

Koopmans, R. J., and J. Molenaar, ''The ''sharkskin-effect'' in polymer extrusion,'' Proc. SPE ANTEC Joint international symposium on structure development in polymers, Indianapolis, Indiana, May 6–9, 1996.

Kurtz, S. J., ''Die geometry solutions to sharkskin melt fracture,'' in *Advances in Rheology*, edited by B. Mena, A. Garcia-Rejon, and C. Rangel-Nafaile, Universidad Nacional Autonoma de Mexico, 1984, pp. 399–407.

Kurtz, S. J., ''The control of sharkskin patterns in film extrusion,'' SPE ANTEC'93, pp. 454–456.

Mackley, M. R., R. P. G. Rutgers, and D. G. Gilbert, ''Surface instabilities during the extrusion of linear low density polyethylene,'' J. Non-Newtonian Fluid Mech. **76**, 281–297 (1998a).

Mackley, M. R., R. P. G. Rutgers, and D. G. Gilbert, ''Surface instabilities during extrusion of linear low density polyethylene,'' in *Dynamics of Complex Fluids*, edited by Adams, Mashelkar, Pearson, and Rennie (Imperial College Press, 1998b), Chap. 1.

McLeish, T. C. B., ''Stability of the interface between two dynamic phases in capillary flow of linear polymer melts,'' J. Polym. Sci., Part B: Polym. Phys. **25**, 2253–2264 (1987).

Piau, J.-M., N. El Kissi, F. Toussaint, and A. Mezghani, ''Distortions of polymer melt extrudates and their elimination using slippery surfaces,'' Rheol. Acta **34**, 40–57 (1995).

Ramamurthy, A. V., ''Wall slip in viscous fluids and influence of materials of construction,'' J. Rheol. **30**, 337–357 (1986).

Renardy, Y. Y., ''Spurt and Instability in a two-layer Johnson-Segalman liquid,'' Theor. Comput. Fluid Dyn. **7**, 463–475 (1995).

Rutgers, R. P. G., ''An experimental and numerical study of extrusion surface instabilities for polyethylene melts,'' Ph.D., University of Cambridge, UK, 1998.

Shore, J. D., D. Ronis, L. Piche, and M. Grant, ''Theory of melt fracture instabilities in the capillary flow of polymer melts,'' Phys. Rev. E **55**, 2976–2992 (1997).

Sornberger, G., J. C. Quantin, R. Fajolle, B. Vergnes, and J. F. Agassant, ''Experimental study of the sharkskin defect in linear low density polyethylene,'' J. Non-Newtonian Fluid Mech. **23**, 123–135 (1987).

Tordella, J. P., ''Unstable flow of molten polymers: A second site of melt fracture,'' J. Appl. Polym. Sci. **7**, 215–229 (1963).

Tremblay, B., ''Sharkskin defects of polymer melts: The role of cohesion and adhesion,'' J. Rheol. **35**, 985–998 (1991).

Tzoganakis, C., B. C. Price, and S. G. Hatzikiriakos, ''Fractal analysis of the sharkskin phenomenon in polymer melt extrusion,'' J. Rheol. **37**, 355–366 (1993).

Venet, C., ''Proprietes d'ecoulement et defauts de surface de resines polyethylenes,'' Ph.D., Ecole Superieure des Mines de Paris, 1996.

Venet, C. and B. Vergnes, ''Experimental characterisation of sharkskin in polyethylenes,'' J. Rheol. **41**, 873–892 (1997).

Vinogradov, G. V., N. I. Insarova, B. B. Boiko, and E. K. Borisenkova, ''Critical regimes of shear in linear polymers,'' Polym. Eng. Sci. **12**, 323–334 (1972).

Wagner, M. H., ''Analysis of time-dependent non-linear stress-growth data for shear and elongational flow of a low-density branched polyethylene melt,'' Rheol. Acta **15**, 136–142 (1976).

Wagner, M. H., ''Zur netzwerktheorie von polymer-schmelzen,'' Rheol. Acta **18**, 33–50 (1979).

Wagner, M. H., A. Bernnat, and V. Schulze, ''The rheology of fibre spinning,'' Kautchuk Gummi Kunststoffe **50**(9), 653–659 (1997).

Wang, S.-Q., P. A. Drda, and Y.-W. Inn, ''Exploring molecular origins of sharkskin, partial slip, and slope change in flow curves of linear low density polyethylene,'' J. Rheol. **40**, 875–898 (1996).

Wang, S. Q. and N. Plucktaveesak, ''Self-oscillations in capillary flow of entangled polymers,'' J. Rheol. **43**, 453–460 (1999).

Watson, J., ''Letter to the Editor: The mystery of the mechanism of sharkskin,'' J. Rheol. **43**, 245–247 (1999a).

Watson, J. M., ''Letter to the Editor: The mystery of the mechanism of sharkskin—Closing remarks by Watson,'' J. Rheol. **43**, 252–252 (1999b).

Wilson, H. J. and J. M. Rallison, ''Short wave instability of co-extruded elastic liquids with matched viscosities,'' J. Non-Newtonian Fluid Mech. **72**, 237–251 (1997).